Heliyon 9 (2023) e13286

Contents lists available at ScienceDirect

Heliyon

journal homepage: www.cell.com/heliyon

Research article

Ag doped Co_3O_4 nanoparticles for high-performance supercapacitor application

Asab Fetene Alem [a], Ababay Ketema Worku [a,*], Delele Worku Ayele [a,b,***], Tessera Alemneh Wubieneh [c], Alebel abebaw Teshager [d], Tadele mihret kndie [d], Bimrew Tamrat Admasu [e], Minbale Admas Teshager [b], Addisu Alemayehu Asege [c], Mehary Dagnew Ambaw [f], Misganaw Alemu Zeleke [c], Alemayehu Kifle Shibesh [d], Temesgen Atnafu Yemata [d,**]

[a] Bahir Dar Energy Center, Bahir Dar Institute of Technology, Bahir Dar University, P.O. Box 26, Bahir Dar, Ethiopia
[b] Department of Chemistry, College of Science, Bahir Dar University, P.O. Box 79, Bahir Dar, Ethiopia
[c] School of Materials Science and Engineering, Bahir Dar University, P.O. Box 79, Bahir Dar, Ethiopia
[d] Faculty of Chemical and Food Engineering, Bahir Dar Institute of Technology-Bahir Dar University, P.O. Box 26, Bahir Dar, Ethiopia
[e] Faculty of Mechanical Engineering, Bahir Dar Institute of Technology-Bahir Dar University, P.O. Box 26, Bahir Dar, Ethiopia
[f] Department of Industrial Chemistry, College of Science, Bahir Dar University, P.O. Box 79, Bahir Dar, Ethiopia

ARTICLE INFO

Keywords:
Doping
Cobalt oxide
Nanoparticles
Co-precipitation method
Supercapacitor

ABSTRACT

Ag doped Co_3O_4 nanoparticles (NPs) were synthesized via a co-precipitation method changing the concentration of Ag. The crystal structure, morphology, surface area, functional group, optical band gap, and thermal property were investigated by XRD, SEM, BET, FTIR, UV–Vis, and TGA/DTA techniques. The XRD results showed the formation of single-cubic Co_3O_4 nanostructured materials with an average crystal size of 19.37 nm and 12.98 nm for pristine Co_3O_4 and 0.25 M Ag-doped Co_3O_4 NPs. Morphological studies showed that pristine Co_3O_4 and 0.25 M Ag-doped Co_3O_4 NPs having a porous structure with small spherical grains, porous structures with sponge-like structures, and loosely packed porous structures, respectively. The pristine and 0.25 M Ag-doped Co_3O_4 NPs showed BET surface areas of 53.06 m^2/g, and 407.33 m^2/g, respectively. The band gap energy of Co_3O_4 NPs were 2.96 eV, with additional sub-bandgap energy of 1.95 eV. Additionally, it was discovered that the band gap energies of 0.25 M Ag-doped Co_3O_4 NPs ranged from 2.2 to 2.75 eV, with an extra sub-band with energies ranging from 1.43 to 1.94 eV for all as-prepared samples. The Ag-doped Co_3O_4 as prepared samples show improved thermal properties due to the doping effect of silver. The CV test confirmed that the 0.25 M Ag-doped Co_3O_4 NPs exhibited the highest specific capacitance value of 992.7 F/g at 5 mV/s in a 0.1 M KOH electrolyte solution. The energy density and power density of 0.25 M Ag-doped Co_3O_4 NPs were 27.9 W h/kg and 3816.1 W/kg, respectively.

* Corresponding author.
** Corresponding author.
*** Corresponding author. Bahir Dar Energy Center, Bahir Dar Institute of Technology, Bahir Dar University, P.O. Box 26, Bahir Dar, Ethiopia.
E-mail addresses: workuketema91@gmail.com (A.K. Worku), atnafutemesgen16@gmail.com (T.A. Yemata).

https://doi.org/10.1016/j.heliyon.2023.e13286
Received 9 December 2022; Received in revised form 23 January 2023; Accepted 25 January 2023
Available online 31 January 2023

1. Introduction

The demand for renewable energy sources has increased in recent years with population growth, and thus researchers have a great responsibility to find advanced energy storage devices to solve the shortage of renewable energy sources [1,2]. Recently, more attention has been paid to renewable energy sources, and work with energy storage such as electric batteries, solar cells and supercapacitors has accelerated [3,4]. Among storage devices, supercapacitors have gained wide attention in recent years due to their advantages of fast charge/discharge rates, affordability, environmental-friendly, high specific capacitance, high power density, and long life cycle [5–12]. These exceptional characteristics and supercapacitors make them suitable candidates used in many electronic devices, memory backups, mobile devices, and in the industrial field for energy storage applications [13]. Based on the nature of electrodes and charge storage mechanisms supercapacitors were categorized into electric double-layer capacitors (EDLC) and pseudocapacitors [14–16]. In EDLCs energy is stored and charge builds up at the interface between the electrode and the electrolytes [17–20], but, in the case of pseudocapacitors, energy is stored by a rapid and reversible faradaic redox reaction [21–24]. Therefore, the overall performance of a supercapacitor is determined based on the choice of its electrode material [25]. For the best results, researchers are currently working on selecting suitable electrode materials for pseudocapacitors applications [26,27]. Transition metal oxides as redox-based electrode materials are the best choice to use for this type of supercapacitor due to their excellent properties such as multiple oxidation states, efficient discharge cyclic ability, and other excellent properties for electrochemical performance [28]**.** As supercapacitors electrode material, transition metal oxides mainly include CeO_2 [29], MnO_2 [30], NiO [31], Fe_2O_3 [32] and Co_3O_4 [33]. Among these transition metal oxides,Co_3O_4 is cost-effective, environmentally friendly, and offers a high theoretical specific capacitance of 3560 F/g [34–36]. Unfortunately, the capacitance of Co_3O_4 in practical applications is quite different from the theoretical value. One reason is that electron transfer is hindered by poor conductivity, limited surface area, large volume expansion and contraction, and strong particle aggregation, resulting in the capacitance and cyclic efficiency of Co_3O_4 are limited [37,38]. The aforementioned disadvantages of Co_3O_4 result in slow kinetics, lower capacity and poor cycling stability during electrochemical experiments. To date, researchers have developed various strategies to overcome the inherent disadvantages of transition metal oxides [39]. To cope with those problems and enhance the properties of Co_3O_4, researchers can undertake multi-step techniques [40]. Among those techniques is to construct nanostructures, consisting of nanospheres, hollow structures, yolk-shell structures, and porous materials, which assist to make amends for the quantity enlargement all through cycling [41,42]. Another approach is to introduce carbonaceous composites, which now no longer handiest to relieve the volume change, however also are conducive to enhance the electronic conductivity [42,43]. Alternatively, metal doping into Co_3O_4 is likewise one a powerful approach to enhance the electrochemical performance, taking gain of the complementary and synergy among ions [41]. Previous research have confirmed that metal doping is a viable manner to modulate the electronic shape without converting the crystal shape of metal oxides and thereby attaining more desirable conductivity and advanced electroactive sites, leading to incredible electrochemical performance [44–46]. Thus, Co_3O_4 nanostructure materials are synthesized by various methods such as solvothermal [47], Spray pyrolysis the sol-gel method [48], thermal decomposition [49], co-precipitation [50] and hydrothermal [51]. However, these approaches are expensive, require complex instruments, and relatively longer preparation times [52,53]. Among them, the co-precipitation method is advantageous due to its fast, cost-effectiveness, and easy control during production [47,54]. Therefore, the properties and electrochemical performance of nanostructured materials can vary depending on experimental parameters such as synthesized method reaction time, concentration, solvent, raw materials and temperature [55]. Therefore, various researchers tried to optimize its electrochemical properties by alloying with various transition metal ions and it was found to be effective in improving supercapacitor performance [56,57]. For example, G. Li et al. examined that Mn-doped Co_3O_4 nanoneedles on nickel foam as a binder-free electrode for supercapacitor applications via a one-step hydrothermal method and demonstrated that the doping of Mn atoms can enhance the electrochemical activity of Co_3O_4 as well as improve the conductivity and outstanding cycling stability of Co_3O_4 with a high specific capacitance of 668.4 F/g at a current density of 1 A/g [58]. Similarly, Uma Sudharshini et al. investigated that 3% Cu-doped Co_3O_4 nanostructure materials were successfully synthesized at a lower temperature of 140 °C using different dopant concentrations via a solvothermal method and exhibited a higher specific capacity value of 812 F/g at a scan rate of 5 mV/s [59]. Similarly, Ali and Khalid. Reported that 5% Sn-doped Co_3O_4 nanorods were successfully synthesized by a solvothermal technique followed by calcination at different temperature ranges (250–400 °C) and showed that the highest specific capacitance was obtained at 350 °C calcination, which was 913.10 F/g [60]. Ali, Khalid, Tahir et al. Studied that the 4% Sb doped Co_3O_4-based electrode material prepared by hydrothermal method achieved a higher specific capacitance of 89.15 F/g at 5 mV/s investigated that 4%Sb doped Co_3O_4 based electrode material produced by a hydrothermal method has achieved a higher specific capacitance of 894.15 F/g at 5 mV/s [61]. Moreover, Khalid et al. reported that 5% Mo-doped Co_3O_4 porous nanostructure materials with different molybdenum concentrations were successfully synthesized through a simple sol–gel method and showed good conductivity and excellent specific capacitance of 858.09 F/g at a scan rate of 5 mV/s [62]. Hence, Ag-doped Co_3O_4 nanostructure materials were found to be mainly used as photocatalytic activities/electrolytes [63–65], Non-Enzymatic Glucose Sensor [66], supercapacitors [67], gas sensors [68], and some other applications. Different studies have been done on the fabrication of Co_3O_4 nanomaterials with alloys such as Cr, Mo, Cu, Fe, Ni, Ag, Sn and Mn, etc. Silver doping improves the electrochemical properties of some other materials has been reported in the literature, but no one has so far reported Ag-doped Co_3O_4 nanostructured materials synthesized by co-precipitation method for supercapacitor applications. Hence, Ag-doped Co_3O_4 NPs were prepared for the first time for a supercapacitor application with a simple method.

2. Experimental methods

2.1. Chemical reagents

All chemicals and reagents were used without any further purification and of analytical grade. Ammonia solution (NH_3, 99.2%), Cobalt chloride Hexahydrate ($CoCl_2$. $6H_2O$, 99.9%), and silver nitrate ($AgNO_3$, 99.9%) were obtained from chemical markets. The solutions were prepared by using distilled water.

2.2. Synthesis of Ag-doped Co_3O_4 NPs

Silver doped-Co_3O_4 NPs were synthesized using a facile co-precipitation technique. In a typical synthesis, 0.3 M of Cobalt chloride hexahydrate ($CoCl_2{\cdot}6H_2O$) and the preferred mole of (0.05, 0.1, 0.15, 0.2, and 0.25 M) silver nitrate ($AgNO_3$, 99.9%) were dissolved in 100 mL distilled water. Then, the resulting mixture was stirred using magnetic stirrer at 80 °C for 3 h. The pH of the mixture was adjusted to 9 by adding 0.2 M NH_3 solution dropwise to the combination of $AgNO_3$. Then, both products was filtered and washed with distilled water and ethanol several times. And the samples were dried in oven at temperature of 100 °C for 6 h to evaporate water and organic materials. Finally, the products were calcined in a muffle furnace at 500 °C for 4 h. A similar method was used to prepare un-doped Co_3O_4. The detailed schematic illustration of Ag-doped Co_3O_4 nanostructured materials prepared by the co-precipitation method is shown in Fig. 1.

2.3. Electrode preparation

Glassy carbon electrode surface has to be polished first with polishing paper and then polished thoroughly with alumina (Al_2O_3) powder slurry on a polishing cloth mounted on glass plate and then rinse with distilled water to remove alumina particles and other possible contaminants and further with deionized water. Un-doped cobalt and Silver doped cobalt oxide (Ag–Co_3O_4) oxide (Co_3O_4) with concentration of 0.25 M in 0.1 M KOH in 50 mL of volumetric flask has to be prepared by serial dilution from 5 M stock solution of Silver doped cobalt oxide and Un-doped cobalt oxide respectively. Three electrodes (Glassy carbon working electrode, reference Ag/AgCl and Pt auxiliary/counter electrode) are inserted into an electrochemical cell filled with 0.1 M KOH. Then background run need to be scanned. Stirring bar is added on the magnetic stirrer to stir the solution so that there is homogeneity of concentration from the surface of the electrode to the bulk solution. Then CV is scanned from an initial potential of +245 mV–0.0 mV and then from 0.0 mV to +245 mV at a scan rate of 5 mV/s to 100 mV/s. Finally, voltammogram of each CV scan have been labeled and saved.

2.4. Characterization

The functional groups of NPs were identified using Fourier transform infrared spectrometer (FT-IR, FT-IR 6660 (JASCO MODEL)) in the wavenumber range of 4000–500 cm^{-1}. The crystal structure and the phase purity of as prepared NPs were carried out by powder X-ray diffraction (MAXima-X XRD-7000, SHIMADZU). The morphology of the prepared NPs were analyzed using SEM, inspect™ SEM, SEM (INSPECT F50) at different magnifications. Thermal properties were Examine using TGA/DTA analysis. The optical properties were determined by Ultraviolet–Visible spectrophotometer (UV–Vis, Lambda 35 (PerkinElmer)) in the wavelength range of 200–800 nm. The Surface area were determined using Brunner-Emmet-Teller (BET) model Quanta chrome Nova Win (Quanta chrome Instruments version 11.0).

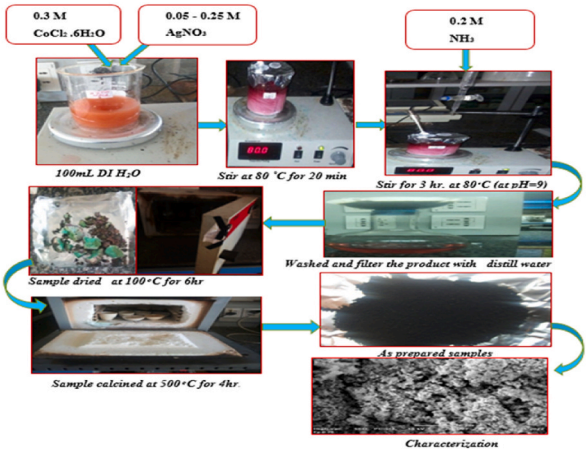

Fig. 1. Synthesis of Ag-doped Co_3O_4 nanostructured materials by Co-precipitation method.

3. Results and discussion

3.1. Structural analysis

The XRD analysis was investigated to determine the structure and crystalline phase of pristine Co_3O_4 and Ag-doped Co_3O_4 NPs. All the prepared samples were examined by XRD technique, and the diffraction peaks as displayed in Fig. 2. The observed XRD peaks around at 2θ are 19.68°, 31.89°, 37.7°, 39.29°, 45.5°, 55.89° and 59.11°, corresponding to (111), (220), (311), (222), (400), (422) and (511) are crystal planes of cubic Co_3O_4, respectively. The XRD peaks are in good agreement with the JCPDS data (JCPDS 09–0 18) [69, 70]. In addition, it was observed that the intensity of the peaks corresponding to the (111), (222), (422), and (511) planes were decreased, while the peaks corresponding to the (220) and (311) increased again. Doping does not affects the bulk structure, but it affects the crystallinity of the materials, the difference in the intensity of the diffraction peaks and the change of peak positions of the samples can be seen. As a result, silver doping increases the crystallinity, due to the variation of the lattice constant. The crystallite size (D) of the nanostructured materials has been estimated using the Debye-Scherer formula (equation (1)) [71].

$$D = \frac{k\lambda}{\beta \cos \theta} \quad (1)$$

Where, "D'' is crystal size, "k" is the Debye–Scherer constant (0.9), "ʎ'' represents the X-ray wavelength used (0.15406 nm), "β" is the width of the peak at half maximum intensity, and "θ" is the diffraction angle, respectively [60]. The average crystallite size was found to be equal to 19.37 and 12.98 nm for pristine Co_3O_4 and 0.25 M Ag-doped Co_3O_4, respectively. The result showed that particle size decreased with silver doping (Table 1). This small crystal value is indicative of the high surface-to-volume ratio that makes them capable of high charge storage.

3.2. SEM analysis

The morphology of pristine, and 0.25 M Ag-doped Co_3O_4 NPs characterized by SEM are shown in Fig. 3 (a-d) with different magnification scales. In Fig. 3(a) SEM morphologies showed that the particles are exhibit porous structure with small spherical grains at magnification scales of 10 μm [72]. Whereas, Fig. 3(b) exhibited a porous structure with sponge like structures at magnification scales of 20 μm. Fig. 3(c) showed that SEM morphologies, a loosely packed porous structure with small cracks/holes at magnification scale of 10 μm. Furthermore, Fig. 3(d) showed flower-like porous morphology at magnification scales of 20 μm. This suggested that, the addition of silver affected the surface morphology of Co_3O_4, as shown in Fig. 3(a–d). It can be seen from the SEM images that there is a clear distinction in morphology between pristine and Ag-doped Co_3O_4 nanostructured materials indicating that the doping concentration of silver has an important influence on the morphology of Co_3O_4 nanostructured materials. Thus, 0.25 M Ag-doped Co_3O_4 NPs show high porosity and better particle dispersion than that of Co_3O_4 nanostructured materials, which is a promising property to enhance the catalytic performance of the as-prepared nanostructure materials. In supercapacitor, this porous structure can offer wide surface area and great specific capacitance [73].

3.3. BET surface area analysis

The specific surface areas, pore volume and pore radius of pristine Co_3O_4 and 0.25 M of Ag-doped Co_3O_4 NPs were determined via the BET analysis [74]. The BET, specific surface area, pore radius, and pore volume of synthesized nanostructure materials are shown in Table 2. The BET specific surface area and corresponding pore volume of the NPs were computed to be (53.066 m^2/g, 0.07425 cc/g) and (407. 33 m^2/g, 0.1153 cc/g) for Co_3O_4 and 0.25 M Ag-doped Co_3O_4 NPs, respectively. Accordingly, 0.25 M Ag-doped Co_3O_4 NPs exhibit the largest BET surface area, which is attributed to the porous structure. Furthermore, the pore radii of Co_3O_4 and 0.25 M Ag–doped Co_3O_4 NPs were to be found 13.85 and 11.56 Å, respectively. Porous structure promotes diffusion and transfer of electrolyte

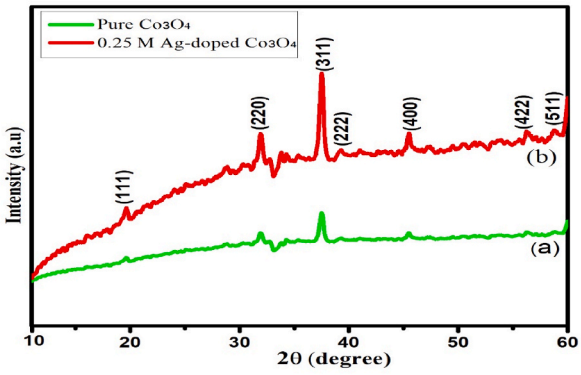

Fig. 2. XRD pattern of (a) Pristine Co_3O_4 nanostructured materials, and (b) 0.25 M Ag-doped Co_3O_4 NPs.

Table 1
XRD results of physical parameters of pristine Co_3O_4, and 0.25 M Ag-doped Co_3O_4 NPs.

Nanostructured materials	2θ	FWHM	D (nm)
Co_3O_4	31.63799	0.42607	19.37945
Ag-doped Co_3O_4	31.63567	0.63583	12.9861

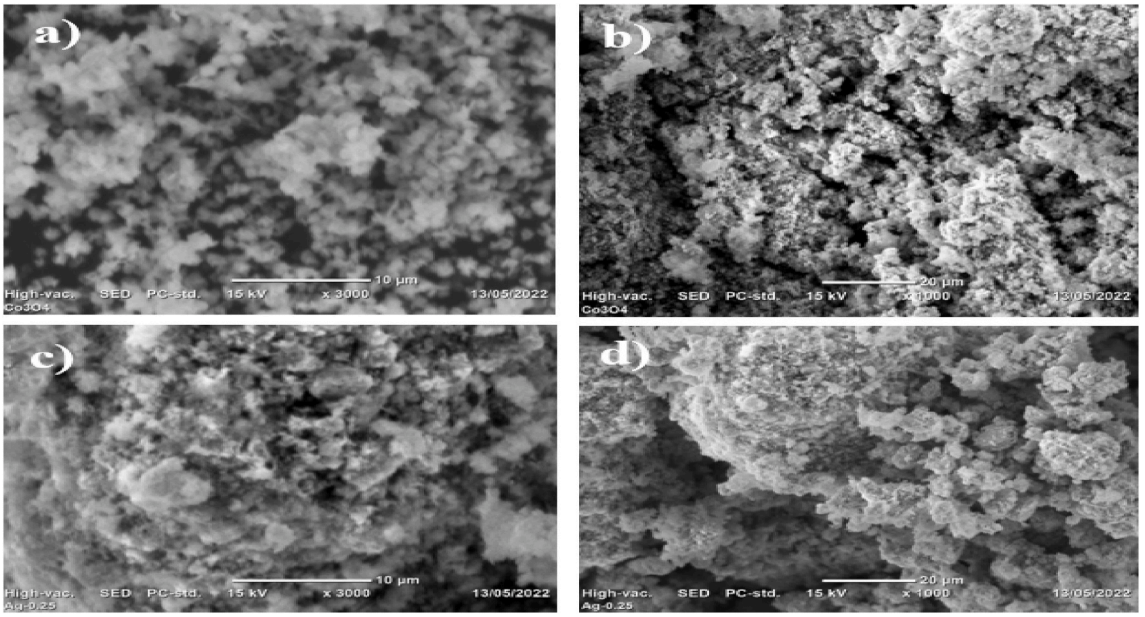

Fig. 3. SEM images of (a) Pristine nanostructured materials at 10 µm, (b) Pristine nanostructured materials at 20 µm, (c) 0.25 M Ag-doped Co_3O_4 nanostructured materials at 10 µm, and (d) 0.25 M Ag-doped Co_3O_4 nanostructured materials at 20 µm.

Table 2
BET specific surface area, pore-volume, and pore radius of Co_3O_4 and Ag-doped Co_3O_4 NPs.

Samples	BET Surface area (m^2/g)	Pore volume (cc/g)	Pore radius (Å)
Co_3O_4	53.066	0.07425	13.85
0.25 M Ag–Co_3O_4	407.338	0.1153	11.56

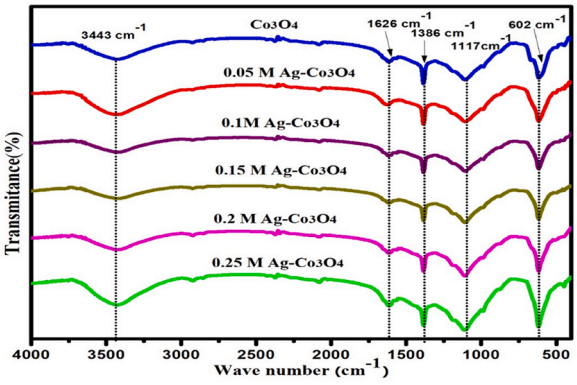

Fig. 4. FTIR spectra of Co_3O_4, Ag-doped Co_3O_4 (0.05 M), Ag-doped Co_3O_4 (0.1 M), Ag- doped Co_3O_4 (0.15 M), Ag-doped Co_3O_4 (0.2 M), Ag-doped Co_3O_4 (0.25 M) NPs.

ions during charge and discharge process [75]. Hence, it was found that the surface area, pore volume and pore size of the Co_3O_4 sample were changed due to the presence of silver ions. In addition, from the SEM images, it can be seen that there is a clear distinction in morphology between pure and Ag-doped Co_3O_4 nanoparticles, indicating that the doping concentration of Ag has an important influence on the morphology of Co_3O_4 nanoparticles. Thus, 0.25 M Ag-doped Co_3O_4 nanoparticles show higher porosity and better particle dispersion than that of Co_3O_4 nanoparticles, which is a promising property to enhance the catalytic performance of the nanoparticles. A good catalytic reaction depends on the morphological characteristics of the material, which means a large surface area, good porosity. Thus, the BET surface area determines the number of active sites available for catalytic activity. As a result, a larger BET surface area is advantageous to the storage and shuttle electrons and ions in the electrode, resulting in a more active site participating for oxidation-reduction reaction leading to improved electrochemical potentials [76].

3.4. FT-IR analysis

FT-IR spectra of un-doped Co_3O_4 and Ag-doped Co_3O_4 NPs were recorded in the range 4000–500 cm^{-1}. Fig. 4 shows the FTIR spectra of Co_3 O_4 and Ag doped Co_3O_4 NPs at various doping levels. As shown Fig. 4, the bands at 3443 cm^{-1} and 1626 cm^{-1} correspond to the O–H stretching and O–H vibration of the adsorbed water molecules, respectively. Moreover, a weak band at 1386 cm^{-1} is due to the presence of residual nitrogen groups that occurred during the combustion technique. Moreover, the band approximately at 1117 cm^{-1} match to the coordination of Co–OH. Finally the characteristic peak at 620 cm^{-1} can be related with the stretching and vibrations of Metal-oxygen bond, which confirms the spinel structure of Co_3O_4. Galini et al. stated that the two characteristic bands obtained for Co_3O_4 nanostructure materials are due to Metal-Oxygen vibrations, confirming the complete decomposition of precursors [77]. UmaSudharshini et al. Stated that the presence of two bands assigned to the vibrations of $Co^{3+}$and Co^{2+} in an octahedral and tetrahedral site, respectively, thereby confirming the formation of the spinel structure Co_3O_4 [59]. The FTIR spectra observed in this study are in a good agreement with previous reported results [59,78,79].

3.5. UV–Vis analysis

UV–Vis measurements were made between 250 and 500 nm to examine the optical properties of the nanostructured materials as they were initially manufactured. The UV–visible spectra of un-doped Co_3O_4 and Ag-doped Co_3O_4 (0.05–0.25 M) NPs is shown in Fig. 5. It was found that when the amount of silver doping increased, the absorbance values in the UV–Visible spectra increased. It may be deduced that silver doping made the Co_3O_4 NPs more optically dense because the level of absorption is a sign of optical density [80]. The existence of two prominent absorption edges in the visible region of all measured spectra, which are attributed to the ligand-to-metal charge transfer event of ($O^{2-} \rightarrow Co^{2+}$) and ($O^{2-} \rightarrow Co^{3+}$) in Co_3O_4, is another intriguing aspect of the absorption spectrum. According to earlier reports in the literature [81]. This suggests the existence of two energy band gaps. With a variation in silver concentration, and Ag-doped Co_3O_4 exhibit different absorption bands. Using the Tauc relation from equation (2) the optical band gap of un-doped Co_3O_4 and Ag-doped Co_3O_4 samples (0.05–0.25 M) was computed [82].

$$(\alpha h\nu)^n = A\left(h\nu - E_g\right) \tag{2}$$

where, A is constant, α is absorption coefficient, hν is photon energy and E_g, is the bandgap energy and n is the constant that is equal to 2, 1/2, 2/3 and 1/3 for allowed direct, allowed indirect, forbidden direct and forbidden indirect transitions, respectively [83]. Fig. 6 (a-f) shows Tauc plot energy bandgap of un-doped Co_3O_4, and Ag-doped Co_3O_4 (0.05, 0.1, 0.15, 0.2 and 0.25 M) nanostructured materials computed by extrapolating the linear part of these plots of $(\alpha h\nu)^2$ axis to ($h\nu$) axis. The Optical bandgap energy results showed below in Table 3.

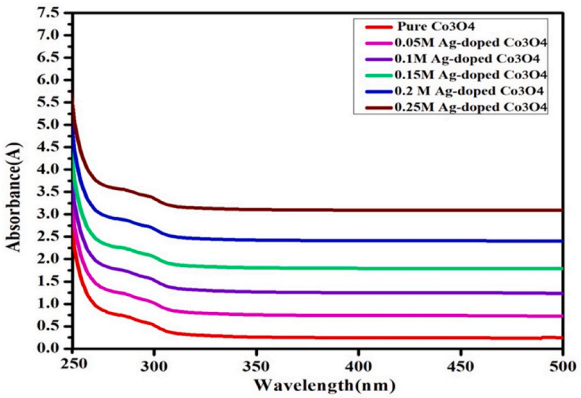

Fig. 5. UV–Vis spectrum of Co_3O_4, Ag-doped Co_3O_4 (0.05 M), Ag-doped Co_3O_4 (0.1 M), Ag-doped Co_3O_4 (0.15 M), Ag-doped Co_3O_4 (0.2 M) and Ag-doped Co_3O_4 (0.25 M) NPs.

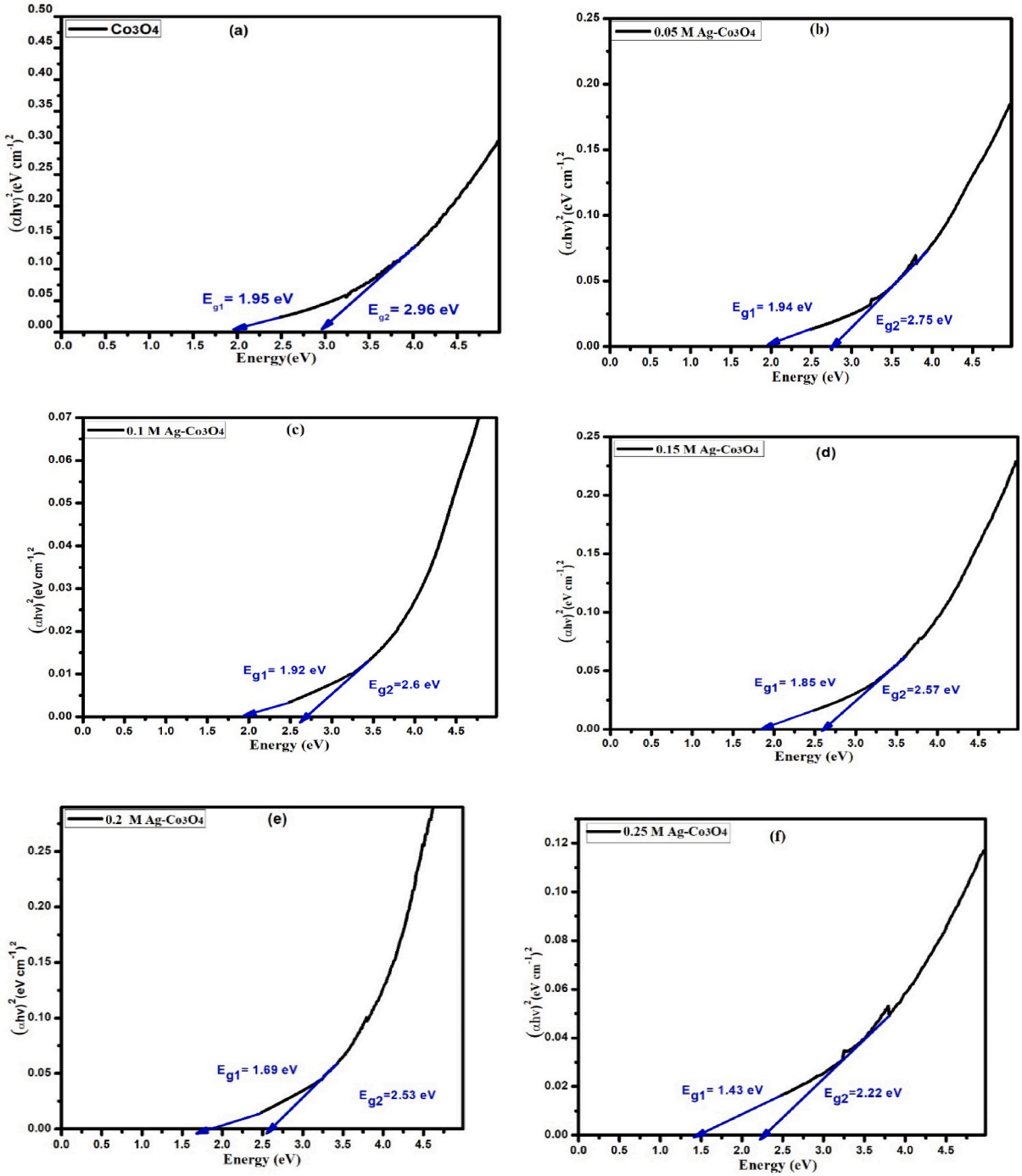

Fig. 6. Tauc plot Bandgap energy of (a) pristine, (b) Ag-doped Co_3O_4 (0.05 M), (c) Ag- doped Co_3O_4 (0.1 M), (d) Ag- doped Co_3O_4 (0.15 M), (e) Ag-doped Co_3O_4 (0.2 M), (f) Ag -doped Co_3O_4 (0.25 M) NPs.

3.6. Thermal (TGA/DTA) analysis

The thermal properties of the pristine and Ag-doped Co_3O_4 NPs were analyzed through TGA and DTA. The sample mass was about 10 mg in a corundum crucible, at a temperature between 25 °C and 900 °C at a heating rate of 20 °C per minute in the air atmosphere. Fig. 7, illustrates the TGA and DTA curves of the Co_3O_4 NPs and Ag- doped Co_3O_4 NPs. The TGA profiles of Co_3O_4 and Ag-doped Co_3O_4 NPs illustrate two stages of weight loss. The first weight loss of 0.37 mg for Co_3O_4 NPs between 25 °C and 262 °C and the corresponding endothermic peak observed at 135 °C may be because of the loss of absorbed water in the sample [67,84,85].

Table 3
Optical band gap values of Co_3O_4 and Ag-doped Co_3O_4 NPs.

Samples	Eg_1 (eV)	Eg_2 (eV)
Co_3O_4 NPs	1.95	2.96
Ag-doped Co_3O_4 (0.05 M)	1.94	2.75
Ag- doped Co_3O_4 (0.1 M)	1.92	2.60
Ag- doped Co_3O_4 (0.15 M)	1.85	2.57
Ag- doped Co_3O_4 (0.2 M)	1.69	2.53
Ag -doped Co_3O_4 (0.25 M)	1.43	2.22

With similar DTA curves at 342 and 506 °C, the second range (1.54 mg) weight loss in the range of 262–599C was connected to the breakdown of the precursor materials or residual organic ligands. The TGA/DTA thermal analysis patterns of Co_3O_4 nanostructured materials, however, show no change after 599C. When heated to 900 °C, the final mass loss of 8.09 mg from the starting weight of 10 mg equals a mass loss of 19.1% (Fig. 7(a)). Similar to this, the first mass loss of 0.4 mg is visible on the 0.05 M Ag– Co_3O_4 TGA curve between 25 and 254 °C, and the endothermic peak that corresponds to this temperature may be caused by the loss of physically adsorbed water (Fig. 7(b)) [67,86]. With matching DTA curves at 398 and 460 °C, the second range (0.13 mg) weight loss in the range of 254–444 °C was connected to the breakdown of residual organic ligands. The TGA/DTA thermal analysis patterns of 0.05 M Ag–Co_3O_4 NPs, however, show no change after 444 °C. When heated to 900 °C, the final mass loss of 9.47 mg from the starting weight of 10 mg is 5.3% mass loss (Fig. 7(b)). Additionally, the first mass loss of 0.36 mg between 25 and 260 °C is visible on the 0.25 M Ag–Co_3O_4 TGA curve, and the endothermic peak at 105 °C that corresponds to it may be caused by the loss of physically adsorbed water (Fig. 7(c)).

With matching DTA curves at 338 and 445 °C, the second range (0.12 mg) weight loss in the 260–415 °C range was connected to the breakdown or residual organic ligands. The TGA/DTA thermal analysis patterns of 0.25 M Ag– Co_3O_4 NPs, however, show no change after 415 °C. When heated to 900 °C, the ultimate mass loss of 9.52 mg from the starting weight of 10 mg is a mass loss of 4.8% (Fig. 7 (c)). Due to the synergetic effects of Ag and Co_3O_4, the material exhibits quite varied thermal properties, according to thermal study. Hence, compared to virgin Co_3O_4, Ag-doped Co_3O_4 NPs exhibit substantially greater thermal stability.

3.7. Capacitive performance analysis

3.7.1. Cyclic voltammetry (CV) study

Electrochemical investigation were performed using cyclic voltammetry (CV). The electrochemical device consists of three electrodes with an electrolyte of 0.1 M KOH. Thus, analysis were applied for the investigation of capacitive characteristics of as-prepared pristine Co_3O_4 and 0.25 M Ag-doped Co_3O_4 nanostructured materials. Moreover, the CV curve were recorded in the potential range of 0.0 to +0.8V versus Ag/AgCl at a scan rate of 5, 10, 20, 50 and 100 mV/s and results are shown in Fig. 8 (a-c). Figure 8(a) shows the comparative CV curve of Co_3O_4, and 0.25 M Ag-doped Co_3O_4 nanostructured materials at a scan rate of 50 mV/s. Thus, the shape of the CV curves for Co_3O_4 and 0.25 M Ag-doped Co_3O_4 nanostructured materials shows a different shape and potential widow. Figure 8(b) shows the detailed CV curves of Co_3O_4 at different scan rates. As the scan rate was increased from 5 to 100 mV/s, the oxidation peak shifted from 0.41 to 0.49 V and the reduction peaks shifted from 0.25V to 0.2 V towards a higher and lower potential. Moreover, Figure 8(c) illustrates the CV curve of 0.25 M Ag-doped Co_3O_4 nanostructured materials. As the scan rate increased from 5 to 100 mV/s, the oxidation peak shifts from 0.28 to 0.34 V and the reduction peaks shifted from 0.134 V to 0.07 V towards a higher and lower potential, respectively, indicating an increase in internal resistance and a polarization effect at a higher scan rate [87]. Furthermore, the wide and sharp redox peaks have been seen from the nonlinear CV curves revealed that the pseudo-capacitance properties of the as-prepared Ag-doped Co_3O_4 nanostructured materials. The anode and cathode peaks are clearly visible. The sharp redox peaks were observed uniform during scanning rate increases from 5 to 100 mV/s, indicating good reversibility of redox reactions [88].

The specific capacities offered by Co_3O_4 and 0.25 M Ag-doped Co_3O_4 NPs were estimated by using the integral charge during the anodic/cathodic scan. The specific capacitance of pristine Co_3O_4 and 0.25 M Ag-doped Co_3O_4 nanostructured materials obtained from CV curves was estimated by employing equation (3) [89].

$$C_s = \frac{\int_{v1}^{v2} IdV}{mv\Delta V} \tag{3}$$

where Cs is the specific capacitance (F/g), I represents the oxidation/reduction current for a given voltage V (v), V_1 is the lower potential limit, V_2 is the upper potential limit, v is the scan rate (v/s), and m is the mass of the electrode. According to the estimation, Co_3O_4 nanostructured materials electrode shows high specific capacitance values of 393.6, 328.7, 230.6, 143.1 and 109.8 F/g at scan rates of 5, 10, 20, 50 and 100 mV/s, respectively. Furthermore, 0.25 M Ag-doped Co_3O_4 nanostructured materials shows high specific capacitance values of 992.7, 757.8, 523.5, 289.3, and 249.7 F/g at the a scan rates of 5, 10, 50 and 100 mV/s,respectively. Hence, 0.25 M Ag Co_3O_4 NPs exhibits only high a specific capacitance value of 992.7 F/g at the scan rates of 5 mV/s (Fig. 9). It can be seen that specific capacities of 0.25 M Ag Co_3O_4 NPs were higher than from recently reported results (Table 4 [35,58–61,81,90–99]) [59]. As a result at slow scanning rate, the movement of ions around the inner and outer surfaces of the prepared nanostructured materials, which

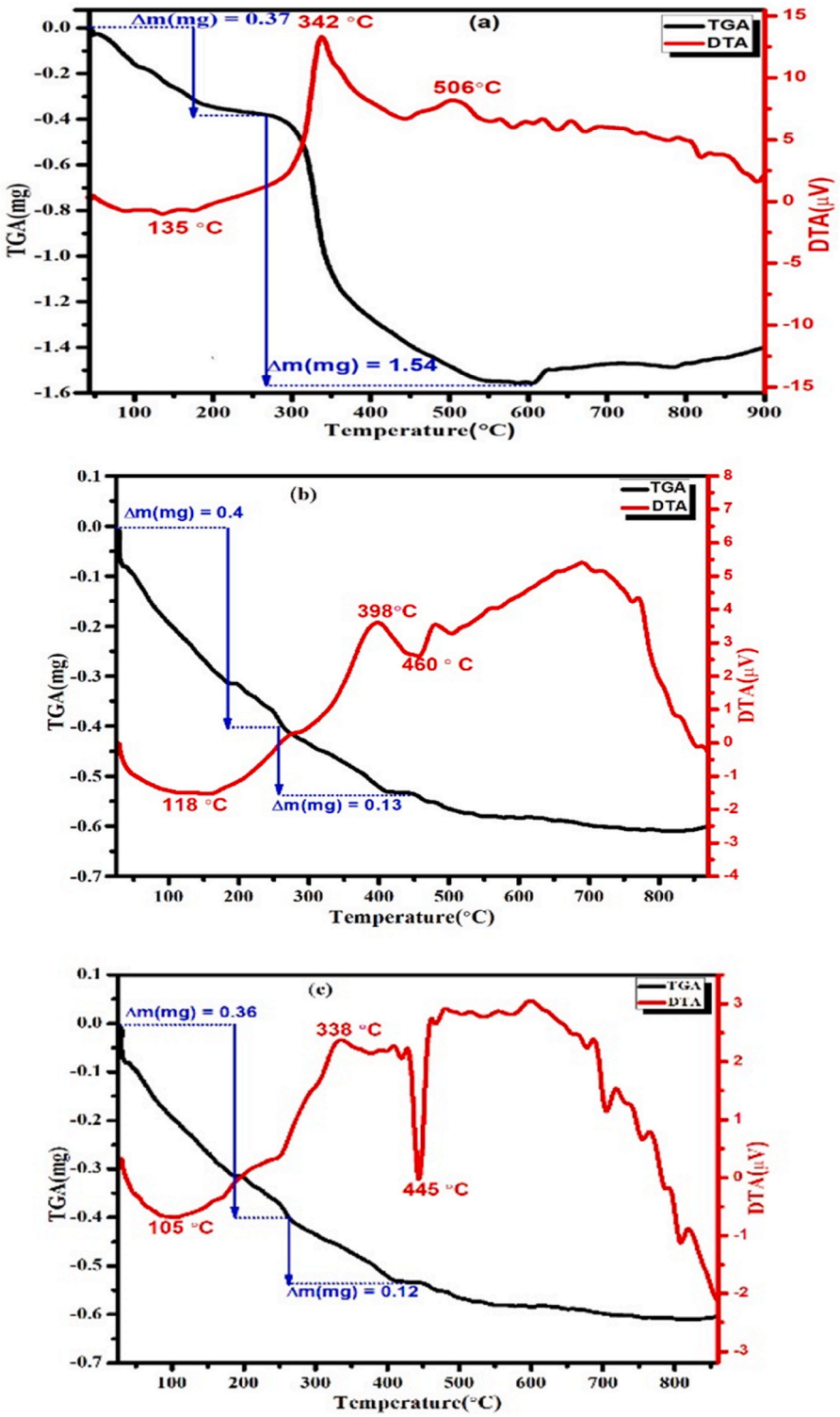

Fig. 7. TGA and DTA curve of (a) Co_3O_4 nanostructured materials, (b) Ag-doped Co_3O_4 (0.05 M) nanostructured materials, and (c) Ag-doped Co_3O_4 (0.25 M) NPs.

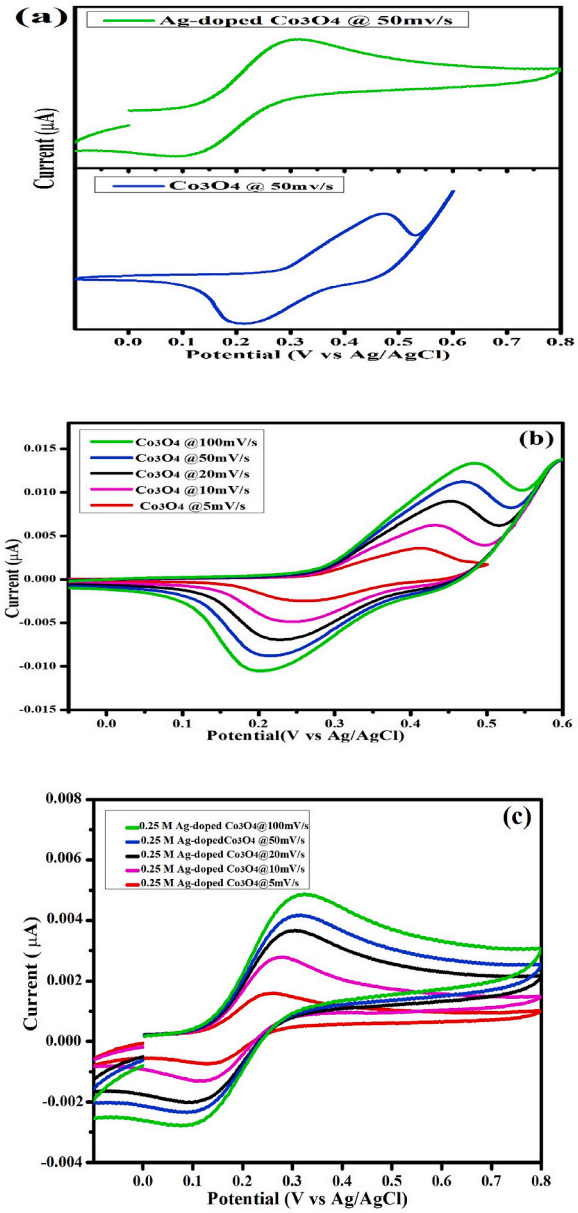

Fig. 8. CV Curve of (a) Co_3O_4 and 0.25 M Ag-doped Co_3O_4 nanostructured materials at 50 mV/s, (b) Co_3O_4 nanostructured materials at different scan rates, and (c) 0.25 M Ag-doped Co_3O_4 nanostructured materials at different scan rates.

makes it possible to obtain a high specific capacity [100].

3.8. Energy and power density analysis

The energy and power density are two key parameters to evaluate the electrochemical performance of supercapacitors. We cannot find the energy density and power density directly from the 3-electrode system because the specific capacitance of the 3-electrode system is four times that of the 2-electrode system. Therefore, to calculate the energy density of a three-electrode system, divide the three-electrode capacitance by four. The energy density and power density of the pristine Co_3O_4 and 0.25 M Ag-doped Co_3O_4 nanostructured materials were obtained according to equations (4) and (5) [101–103].

$$\mathbf{E} = \frac{\mathbf{1}}{\mathbf{2}} \boldsymbol{C} (\Delta \boldsymbol{V})^{\mathbf{2}} \Big/ \mathbf{3.6} \tag{4}$$

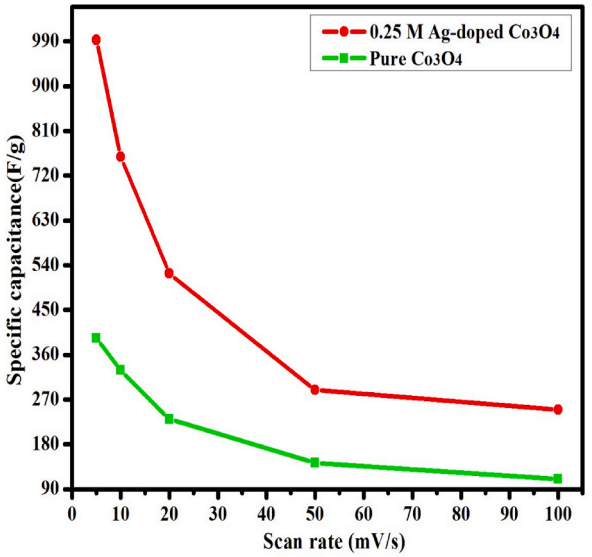

Fig. 9. The values of specific capacitance versus scan rate for pristine Co_3O_4, and 0.25 M Ag-doped Co_3O_4 NPs.

Table 4
Comparison of specific capacities of various metal-doped Co_3O_4 NPs reported in literatures.

Materials	Specific capacitance	Scan rate	Electrolyte	Synthesis method	Reference
0.4 Sn doped Co_3O_4 nanowires	151.8 F/g	5 mV/s	6 M KOH	Hydrothermal method	[90]
Co_3O_4nanopowdes	291 F/g	10 mV/s	2 M KOH	Chemical reduction method	[91]
Hydrophilic Co_3O_4	315 F/g	5 mV/s	0.5 MNa_2SO_4	Galvanostatic electrodeposition	[92]
1% Mn-doped Co_3O_4 thin film	675 F/g	10 mV/s	0.1 M KOH	Sol–gel spin coat deposition	[93]
3% B-doped Co_3O_4 thin films	482.35 F/g	5 mV/s	6 M KOH	Spray deposition method	[94]
Ag-doped Co_3O_4 nanorods	584 F/g	5 mV/s	1 M KOH	Hydrothermal route method	[95]
Mn-doped Co_3O_4 nanoneedles	668.4 F/g	1 A/g	2 M KOH	one-step hydrothermal reaction	[58]
Ru:Co_3O_4 thin electrodes	628.33 F/g	1 mV/s	1 M KOH	Spray pyrolytic deposition	[96]
5% Cd doped porous Co_3O_4 nanosheet	737 F/g	A/g	6 M KOH	Co-precipitation method	[97]
2.5% Fe:Co_3O_4 thin films	429 F/g	2 mV/s	1 M KOH	Nebulizer spray pyrolysis	[81]
3% Cu-doped Co_3O_4 nanostructure materials	812 F/g	5 mV/s	6 M KOH	solvothermal method	[59]
Mn-doped Co_3O_4 oblique prisms	909 F/g	1 A/g	2 M KOH	Solvothermal reaction	[35]
Au - doped Co_3O_4	763 F/g	1 A/g	2 M KOH	Calcining Au@ZIF-67.	[98]
5%Sn-doped Co_3O_4 nanorods	842.44 F/g	5 mV/s	3 M KOH	Solvothermal method	[60]
5% Mo-doped Co_3O_4 Nanostructure materials	858.09 F/g	5 mV/s	3 M KOH	Sol-gel method	[42]
4%Sb-doped Co_3O_4 electrode	894.15 F/g	5 mV/s	3 M KOH	Hydrothermal method	[61]
Urchin-like Fe-doped Co_3O_4 microstructures	315.8C/g	1 A/g	2 MKOH	Hydrothermal method	(S [99].
0.25 M Ag-doped Co_3O_4 NPs	992.7 F/g	5 mV/s	0.1 M KOH	Co-precipitation method	This work

$$\mathbf{P = 3600\ E/\Delta t} \tag{5}$$

where, E, C, ΔV, P and Δt is the energy density (Wh/kg), capacitance of the electrode (F/g), potential window of device, power density (W/kg), and discharge time, respectively. The maximum energy density of the Co_3O_4 nanostructured materials was 6.69 W h/kg at a power density of 160.4 W/kg. Whereas, 0.25 M Ag doped Co_3O_4 nanostructured materials was 9.17 W h/kg at a power density of 472.1 W/kg. The power density of pristine Co_3O_4 and 0.25 M Ag-doped Co_3O_4 NPs in this study was higher than previously stated values in the literature [104].

4. Conclusion

In conclusion, pristine and Ag-doped Co_3O_4 NPs were successfully prepared via the Co-precipitation method with various doping concentration. XRD pattern confirmed the unchanged crystal structures of Co_3O_4 and the decrease in crystallite size with the addition of dopant Ag. SEM confirmed the formation of structures having porous structure with small spherical grains, porous structures with sponge-like structures, loosely packed porous structures with small cracks/holes, and flower-like porous morphology, respectively. Pristine Co_3O_4 and 0.25 M Ag-doped Co_3O_4 nanostructured materials have BET surface areas of 53.06 m^2/g, and 407.338 m^2/g, respectively. The bandgap energy values of Co_3O_4 nanostructured materials were 2.96 eV, with an additional sub-band gap energy of

1.95 eV. Furthermore, the band gap energies of Ag-doped Co_3O_4 nanostructured materials were found to be between 2.22 and 2.75 eV for all samples, with an additional sub-band corresponding to energies varying between 1.43 and 1.94 eV. The bandgap energy decreased with increasing Ag doping concentration and the obtained bandgap energy range confirmed the semiconducting nature of the prepared Ag-doped Co_3O_4 NPs. The presence of M−O bonds (M = Co, Ag) was analyzed by FTIR spectroscopy. The Ag-doped Co_3O_4 NPs show improved thermal properties owing to the doping effect of silver ions. The electrochemical study were done with the help of CV analysis in a 0.1 M KOH electrolyte solution. The influence of Ag concentration on the capacitance characteristics of Co_3O_4 nanostructured material was tested by conducting CV. In comparison to other pristine and Ag-doped Co_3O_4 samples, the 0.25 M Ag-doped Co_3O_4 sample showed the highest specific capacitance values of 992.7 F/g at a scan rate of 5 mV/s, due to its larger surface area from the reduced particle size. The TGA result confirmed that Ag-doped Co_3O_4 nanostructured materials show much stronger thermal stability than Co_3O_4 nanostructured materials. Furthermore, the energy density and power density of the Co_3O_4 and 0.25 M Ag-doped Co_3O_4 nanostructured materials were 6.69 W h/kg, 160.4 W/kg, and 27.9 W h/kg, 3816.1 W/kg, respectively.

Author contribution statement

Asab Fetene Alem, Ababay Ketema Worku: Conceived and designed the experiments; Performed the experiments; Analyzed and interpreted the data; Wrote the paper.

Temesgen Atnafu Yemata, Delele Worku Ayele, Nigus Gabbiye Habtu: Analyzed and interpreted the data; Contributed reagents, materials, analysis tools or data; Wrote the paper.

Tessera Alemneh Wubieneh, Alebel abebaw, Tadele mihret kndie, Bimrew Tamrat Admasu, Minbale Admas Teshager, Addisu Alemayehu Asege, Mehary Dagnew Ambaw, Misganaw Alemu Zeleke, Alemayehu Kifle Shibesh: Conceived and designed the experiments; Wrote the paper.

Funding statement

This research did not receive any specific grant from Funding agencies in the public, commercial, or not-for-profit sectors.

Data availability statement

Data will be made available on request.

Declaration of interest's statement

The authors declare no conflict of interest.

Acknowledgments

The authors thank the grant from the postgraduate office. Faculty of Chemical and Food Engineering is acknowledged for the laboratory chemicals, materials, and instruments funding.

References

[1] Ababay Ketema Worku, Delele Worku Ayele, Nigus Gabbiye Habtu, Minbale Admas Teshager, et al., Enhancing oxygen reduction reaction activity of ε-MnO2 nanoparticles via iron doping, J. Phys. Chem. Solid. 157 (June) (2021).
[2] Wenhua Zuo, et al., A novel phase-pransformation ectivation process toward Ni–Mn–O ranoprism zrrays for 2.4 V ultrahigh-voltage nqueous supercapacitors, Adv. Mater. 29 (36) (2017) 1–9.
[3] A.K. Worku, D.W. Ayele, N.G. Habtu, Recent tdvances and auture nerspectives in angineering of uifunctional alectrocatalysts for aechargeable finc–air batteries, Materials Today Advances 9 (2021), 100116.
[4] A.A. Yadav, A.C. Lokhande, J.H. Kim, C.D. Lokhande, High electrochemical performance esymmetric supercapacitor based on La2O3//Co3O4 electrodes, J. Ind. Eng. Chem. 56 (2017) 90–98.
[5] Wang Chen, et al., One Step Hydrothermal Synthesis of Flower-Shaped Co 3 O 4 Nanorods on Nickel Foam as Supercapacitor Materials and Their Excellentnce, 2018, p. 1606.
[6] Yong Ping Gao, et al., Cycling profile of layered MgAl2O4/reduced eraphene oxide composite for rsymmetrical supercapacitor, J. Colloid Interface Sci. 539 (2019) 38–44.
[7] Xiaoyi Hou, et al., Ultrathin ZnS zanosheet/carbon nanotube aybrid electrode for high-performance flexible all-golid-atate supercapacitor, Nano Research 10 (8) (2017) 2570–2583.
[8] Kowsik Sambath Kumar, et al., High-performance nlexible nsymmetric supercapacitor based on RGO anode and WO3/WS2core/shell hanowire cathode, Nanotechnology 31 (43) (2020).
[9] Liu Yumeng, Imran Murtaza, Shujia Ahmed, Hong Meng, Interfacial fodification for seightening the snteraction between PEDOT and fubstrate towards enhanced alexible nolid supercapacitor performance, Chem. Eng. J. 379 (2020) 1–24.
[10] Monalisa Pal, Rupali Rakshit, Ashutosh Kumar Singh, Kalyan Mandal, Ultra high supercapacitance of mltra small Co3O4 hanocubes, Energy 103 (2016) 481–486.
[11] Seoyoon Shin, Moo Whan Shin, Nickel metal–organic sramework (Ni-f) serived NiO/C@CNF composite for the application of high performance uelf-ntanding supercapacitor electrode, Appl. Surf. Sci. 540 (2021), 148295.
[12] Jianhua Yu, et al., Facile synthesis of binary transition metal sulfide fubes moferived from NiCo-MOF-74 for high-performance supercapacitors, Energy Technol. 7 (6) (2019).
[13] Arie Borenstein, Ortal Hanna, Attias Ran, Shalom Luski, Carbon-based composite materials for supercapacitor electrodes : a deview, J. Mater. Chem.: Materials for energy and sustainability 5 (2017) 12653–12672.

[14] Muhammad Aadil, Sonia Zulfiqar, Philips O. Agboola, et al., Fabrication of sraphene supported binary sanohybrid with multiple approaches for electrochemical energy storage applications, Synth. Met. 272 (October 2020) (2021), 116645.
[15] Behnam Chameh, Morteza Moradi, Shaaker Hajati, Fereidon Alikhani Hessari, Design and construction of ZIF(8 and 67) supported Fe3O4 composite as advanced materials of high performance supercapacitor, Phys. E Low-dimens. Syst. Nanostruct. 126 (July 2020) (2021), 114442.
[16] Wensha Niu, et al., Synthesis of nickel tulfide-dupported on porous carbon from a natural reaweed-derived golysaccharide for high-performance supercapacitors, J. Alloys Compd. 853 (2021), 157123.
[17] Yuexin Liu, et al., Acetylene nlack enhancing the electrochemical performance of NiCo-s sanosheets for supercapacitor electrodes, Appl. Surf. Sci. 492 (2019) 455–463.
[18] Maria R. Lukatskaya, et al., Ultra-high-rate pseudocapacitive energy storage in two-simensional transition metal darbides, Nature Energy 17105 (July) (2017) 1–6.
[19] Wenwen Tian, et al., Phytic pcid bodified mofanganese nioxide/draphene composite cerogel as high-performance electrode materials for supercapacitors, Appl. Surf. Sci. (2019), 143589.
[20] Yakun Wang, et al., Nitrogen and ahosphorus Co-doped milkworm-mocoon-based delf-gctivated porous carbon for high performance supercapacitors, J. Power Sources 438 (June) (2019), 227045.
[21] Tanut Pettong, et al., High-performance asymmetric supercapacitors of MnCo2O4 panofibers and N-doped reduced sraphene oxide cerogel, ACS Appl. Mater. Interfaces 8 (49) (2016) 34045–34053.
[22] Imran Shakir, Zeyad Almutairi, Sahar Saad, Fabrication of binary transition metal sydroxides and their aanocomposite with CNTs for electrochemical capacitor applications, Ceram. Int. (August) (2020).
[23] Li Sun, Qiang Fu, Chunxu Pan, Mn3O4 ambedded 3D multi-neteroatom godoped carbon aheets/carbon foams composites for high-performance hlexible supercapacitors, J. Alloys Compd. 849 (2020), 156666.
[24] Wen Zhou, et al., Polypyrrole doped with nodecyl eenzene hulfonate electrodeposited on carbon sibers for flexible capacitors with high-performance, Electrochim. Acta 176 (2015) 594–603.
[25] Jiangfeng Li, Guangtao Zan, Qingsheng Wu, An dltra-high-performance anode material for supercapacitors: belf-sssembled long Co3O4 hollow eube fetwork with multiple feteroatom (C-, N- and S-) doping, J. Mater. Chem. 4 (23) (2016) 9097–9105.
[26] Ababay Ketema Worku, Worku Ayele Delele, Gabbiye Habtu Nigus, Atnafu Yemata Temesgen, Engineering Co3O4/MnO2 uanocomposite materials for oxygen reduction slectrocatalysis, Heliyon 7 (9) (2021), e08076. https://www.sciencedirect.com/science/article/pii/S2405844021021794.
[27] Ababay Ketema Worku, Worku Ayele Delele, Gabbiye Habtu Nigus, Admas Teshager Minbale, et al., Recent arogress in MnO2-based oxygen tlectrocatalysts for nechargeable hinc-air batteries, Materials Today Sustainability (2021), 100072. https://linkinghub.elsevier.com/retrieve/pii/S2589234721000130. (Accessed 27 May 2021).
[28] S.V. Khavale, B.J. Lokhande, Electrochemical performance of eotentio-iynamically peposited Co3O4 electrodes: influence of dnnealing temperature, J. Mater. Sci. Mater. Electron. 28 (7) (2017) 5106–5115.
[29] Mengxuan Sun, et al., Electrochimica acta mesoporous Zr-doped CeO 2 nanostructures as auperior supercapacitor electrode with migni si santly enhanced fpeci ci c capacity and excellent cycling stability, Electrochimica Acta 331 (135366) (2020) 1–10.
[30] Muhamed Shareef Kolathodi, Milan Palei, Tirupattur Srinivasan Natarajan, Gurpreet Singh, MnO2 sncapsulated flectrospun TiO2 eanofibers as electrodes for esymmetric supercapacitors, Nanotechnology 31 (12) (2020), 125401.
[31] H.K. Jung, S.J. Lee, D. Han, A.-R. Hong, H.S. Jang, S.H. Lee, D.H. Kim Mun, H. Lee, S.H. Han, D. Yang, Au-incorporated NiO nanocomposite ahin nilms as tlectrochromic electrodes for supercapacitors, J.H. Electrochim. Acta 330 (135203) (2019).
[32] Chenglong Liu, et al., Surface-functionalized Fe2O3 fanowire errays with enhanced pseudocapacitive performance as novel anode materials for high-energy-density aiber-nhaped fsymmetric supercapacitors, Electrochim. Acta 330 (xxxx) (2020), 135247.
[33] Xueying Yang, et al., Co3O4-Doped two-simensional carbon aanosheet as an electrode material for high-performance dsymmetric supercapacitors, Electrochim. Acta 335 (2020), 135611.
[34] Muhammad Aadil, Sonia Zulfiqar, Humera Sabeeh, et al., Enhanced electrochemical energy storage properties of carbon noated Co3O4 nanoparticles-reduced araphene oxide mernary nano-cybrids, Ceram. Int. 46 (11) (2020) 17836–17845.
[35] Huiyu Chen, et al., Facile synthesis of porous Mn-doped Co 3 O 4 oblique prisms as an electrode material with remarkable pseudocapacitance, Ceram. Int. 45 (6) (2019) 8008–8016.
[36] Xiaomin Wang, et al., A tightly packed Co3O4/C&S composite for high-performance electrochemical supercapacitors from a cobalt(III) cluster-based coordination precursor, J. Solid State Chem. 288 (May) (2020), 121435.
[37] Junlin Lu, et al., A facile strategy of in-situ anchoring of Co3O4 on N doped carbon cloth for an ultrahigh electrochemical performance, Nano Res. 14 (7) (2021) 2410–2417.
[38] Xuelei Wang, et al., Recent advance in Co3O4 and Co3O4-containing electrode materials for high-performance supercapacitors, Molecules 25 (2) (2020).
[39] Ababay Ketema Worku, Worku Ayele Delele, Gabbiye Habtu Nigus, Influence of nickel doping on MnO2 nanoflowers as electrocatalyst for oxygen reduction reaction, SN Appl. Sci. 3 (9) (2021), https://doi.org/10.1007/s42452-021-04746-7.
[40] Ababay Ketema Worku, et al., Engineering techniques to tendrite free ainc-based cechargeable batteries, Front. Chem. (September) (2022) 1–15.
[41] Xiaoling Tong, Min Zeng, Jing Li, Liu Zhanjun, Porous Co3O4@TiO2 core-shell panofibers as advanced anodes for lithium ion batteries, 12, 14, J. Alloys Compd. (2017) 16276–16285.
[42] Mingjun Xiao, et al., Ionic vuid nerived Co3O4/n itrogen doped carbon composite as anode of lithium ion b-atteries with enhanced rate performance and cycle stability, J. Mater. Sci. Mater. Electron. (2019), 0(0): 0.
[43] Xin Wu, Min Zeng, Lige Wang, Jing Li, CTAB-assisted synthesis of ZnCo2O4 nanoparticles lmbedded in N-doped carbon as duperior anode materials for lithium-eon sattery, J. Alloys Compd. 780 (2019) 897–906.
[44] Cui Dong, Zhenping Qu, Xiao Jiang, Yewei Ren, Tuning oxygen lacancy concentration of MnO2 through metal doping for improved ioluene oxidation, J. Hazard Mater. 391 (December 2019) (2020), 122181.
[45] Green Energy, et al., Manganese doping to boost the capacitance performance of vierarchical Co 9 S 8 @ Co (OH) 2 tanosheet brrays, Green Energy and Environment (xxxx) (2021), 0–8.
[46] Xiaoyan Han, Yiping Cui, Haowen Liu, Ce-doped Mn 3 O 4 as high-performance anode material for nithium ion batteries, J. Alloys Compd. 814 (2020), 152348.
[47] Jianfang Wang, et al., Synthesis of δ-MnO2/C assisted with carbon aheets by directly carbonizing from lorn stalk for high-performance supercapacitor, Mater. Lett. 285 (2021), 129116.
[48] Manoj Pudukudy, Zahira Yaakob, Sol-gel synthesis, characterisation, and photocatalytic activity of porous spinel Co3O4 canosheets, Chem. Pap. 68 (8) (2014) 1087–1096.
[49] Saeed Farhadi, Masoumeh Javanmard, Gholamali Nadri, Characterization of cobalt oxide nanoparticles prepared by the thermal decomposition of [Co(NH3)5(H2O)](NO3)3 complex and study of their photocatalytic activity, Acta Chim. Slov. 63 (2) (2016) 335–343.
[50] MuhammCad Ramzan Saeed Ashraf Janjua, Synthesis of Co3O4 sano cggregates by Co-precipitation method and its catalytic and nuel additive applications, Open Chemistry 17 (1) (2019) 865–873.
[51] Mahatta Oza, M.J. Joshi, Hydrothermal synthesis of aiderite fano-particles and characterizations, AIP Conf. Proc. 1837 (2017).
[52] Xin Min, et al., Synthesis of MnO2 serived from spent nithium-con batteries via advanced oxidation and its application in VOCs oxidation, J. Hazard Mater. 406 (2021), 124743. http://www.sciencedirect.com/science/article/pii/S0304389420327333.
[53] Tao Peng, et al., Facile synthesis of SiO2@MnO2 danocomposites and their applications on llatforms for iensitively sensing nntibiotics and plutathione, Sensor. Actuator. B Chem. 304 (2020), 127314. http://www.sciencedirect.com/science/article/pii/S0925400519315138.

[54] Xin Fu, et al., Rapid oxidation-stching synthesis of aow-crystalline δ-MnO2 gubular nanostructures under embient with high capacitance, J. Colloid Interface Sci. 557 (2019) 168–173. http://www.sciencedirect.com/science/article/pii/S0021979719310574.

[55] Ababay Ketema Worku, et al., Energy storage lechnologies; recent tdvances, ahallenges, and drospectives, in: Aashish Kumar Bohre, Pradyumn Chaturvedi (Eds.), Planning of Hybrid Renewable Energy Systems, Electric Vehicles and Microgrid: Modeling, Control and Optimization, Mohan Lal Kolhe, and Sri Niwas Singh, Springer Nature Singapore, Singapore, 2022, pp. 125–150, https://doi.org/10.1007/978-981-19-0979-5_7.

[56] Feifei Wang, et al., Co-doped Ni3S2@CNT arrays anchored on graphite foam with a hierarchical conductive network for high-performance supercapacitors and hydrogen evolution electrodes, J. Mater. Chem. 6 (22) (2018) 10490–10496.

[57] Lin Zhu, et al., Lower ammoniation activation energy of CoN nanosheets by Mn doping with superior energy storage performance for secondary ion batteries, Nanoscale 10 (12) (2018) 5581–5590.

[58] Guangmin Li, et al., Manganese doped Co 3 O 4 mesoporous nanoneedle array for long cycle-stable supercapacitors, Appl. Surf. Sci. 469 (2019) 941–950.

[59] A. UmaSudharshini, et al., Solvothermal synthesis of Cu-doped Co3O4 nanosheets at low reaction temperature for potential supercapacitor applications, Appl. Phys. Mater. Sci. Process 127 (5) (2021) 1–11.

[60] Faisal Ali, N.R. Khalid, E ff ect of calcination temperature on structural , morphological and electrochemical properties of Sn doped Co 3 O 4 nanorods, Ceram. Int. 46 (October) (2020) 24137–24146.

[61] Faisal Ali, N.R. Khalid, M.B. Tahir, et al., Capacitive properties of novel Sb-doped Co3O4 electrode material synthesized by hydrothermal method, Ceram. Int. 47 (22) (2021) 32210–32217.

[62] N.R. Khalid, et al., Electrochemical study of Mo-doped Co3O4 nanostructures synthesized by sol–gel method, J. Mater. Sci. Mater. Electron. 32 (3) (2021) 3512–3521.

[63] Muhammad Aadil, Sonia Zulfiqar, Muhammad Farooq Warsi, et al., Mesoporous and macroporous Ag-doped Co3O4 nanosheets and their superior photo-catalytic properties under solar light irradiation, Ceram. Int. 47 (7) (2021) 9806–9817.

[64] Muhammad Saeed, et al., Ag-Co3O4: synthesis, characterization and evaluation of its photo-catalytic activity towards degradation of rhodamine B dye in aqueous medium, Chin. J. Chem. Eng. 26 (6) (2018) 1264–1269.

[65] Kai Li Yan, et al., Mesoporous Ag-doped Co3O4 nanowire arrays supported on FTO as efficient electrocatalysts for oxygen evolution reaction in acidic media, Renew. Energy 119 (2018) 54–61.

[66] Xiao Bai, Ziyin Yang, Synthesis of Ag/Co 3 O 4 for high sensitive non-enzymatic Glucose sensor through synergy of surface/interface engineering, J. Electrochem. Soc. 168 (10) (2021), 107508.

[67] Muhammad Aadil, Sonia Zulfiqar, Muhammad Shahid, et al., Binder free mesoporous Ag-doped Co3O4 tanosheets with outstanding cyclic stability and rate fapability for advanced supercapacitor applications, J. Alloys Compd. (2020), 156062.

[68] R. Molavi, M.H. Sheikhi, Low temperature carbon nonoxide gas sensor based on Ag-Co3O4 thick film ianocomposite, Mater. Lett. 233 (August) (2018) 74–77.

[69] Ayse Kucukarslan, et al., Improvement of structural , optical and magnetic properties of cobalt oxide nhin silms by doping with dron, Appl. Phys. A (2021) 1–9.

[70] Zondi Nate, Atal A.S. Gill, Ruchika Chauhan, Rajshekhar Karpoormath, Polyaniline-cobalt oxide aanofibers for dimultaneous electrochemical petermination of pntimalarial frugs: mrimaquine and froguanil, Microchem. J. 160 (PB) (2021), 105709.

[71] Shyamal Das, C. Manoharan, M. Venkateshwarlu, P. Dhamodharan, Structural, optical, morphological and magnetic properties of nickel doped cobalt cerrite nanoparticles synthesized by hydrothermal method, J. Mater. Sci. Mater. Electron. 30 (22) (2019) 19880–19893.

[72] Singh Avtar, Kumar Davinder, Anup Thakur, Singh Saini Balraj, Enhanced performance of Fe-doped manganese oxide wilms as supercapacitor electrodes, Bull. Mater. Sci. 43 (2020) 1–9.

[73] Tianyu Liu, Guoliang Liu, Block lopolymer-based porous carbons for supercapacitors, J. Mater. Chem. 7 (41) (2019) 23476–23488.

[74] Rumana Hossain, Veena Sahajwalla, Microrecycled Co3O4 from baste cithium-ion mattery: synthesis, bharacterisation and nmplication in environmental application, J. Environ. Chem. Eng. (2022), 107858.

[75] Saeed Ahmed, et al., Effective removal of methylene rlue using sanoscale danganese oxide mods and fpheres aerived from different precursors of sanganese, J. Phys. Chem. Solid. 155 (2021), 110121.

[76] Dhanaji B. Malavekar, et al., Enhanced energy density of alexible tsymmetric folid state supercapacitor device fabricated with dmorphous ehin ailm electrode materials, J. Phys. Chem. Solid. 141 (2020), 109425.

[77] Masumeh Galini, Mehdi Salehi, Mahdi Behzad, Structural, magnetic and mielectric properties of Dy-doped Co 3 O 4 nanostructures for the electrochemical evolution of oxygen in ilkaline media, J. Nanostructures 8 (4) (2018) 391–403.

[78] Reena, R. Sylvia, A. Aslinjensipriya, M. Jose, S. Jerome Das, Investigation on structural, optical and electrical nature of pure and Cr-dncorporated cobalt oxide nanoparticles prepared via Co-precipitation method for photocatalytic activity of aethylene flue dye, J. Mater. Sci. Mater. Electron. 31 (24) (2020) 22057–22074, https://doi.org/10.1007/s10854-020-04708-6.

[79] M. Sundararajan, et al., Study of physical and magnetic properties of Mg:Co3O4 spinels using L-orginine as nuel, J. Ovonic Res. 17 (5) (2021) 479–486.

[80] Huan Chen, et al., Vertically triented carbon fanotube as a stable trame to support the Co0.85Se nanoparticles for high performance supercapacitor electrode, J. Alloys Compd. 855 (2021).

[81] M. Manickam, et al., Structural, optical, electrical and electrochemical properties of Fe:Co3O4 fhin dilms for supercapacitor applications, J. Mater. Sci. Mater. Electron. 28 (24) (2017) 18951–18965.

[82] Abdelmalek Kharoubi, et al., Characterization of Ni-doped TiO2 dhin cilms deposited by uip-toating technique, EPJ Applied Physics 72 (3) (2015) 1–7.

[83] Muslima Zahan, Jiban Podder, Surface morphology, optical properties and trbach fail of Spray deposited Co 3 O 4 chin gilms, J. Mater. Sci. Mater. Electron. 30 (4) (2019) 4259–4269.

[84] Yuhong Jin, et al., Characterization of Porous Micro-/Nanostructured Co3O4 Microellipsoids, Elsevier Ltd, 2015.

[85] Cedrik Ngnintedem Yonti, et al., Green Synthesis of Iron-Doped Cobalt Oxide Nanoparticles from Palm Kernel Oil via Co-precipitation and Structural Characterization, 2021.

[86] Ababay Ketema, Worku Delele, Gabbiye Nigus, Engineering Co 3 O 4/MnO 2 nanocomposite materials for oxygen reduction hlectrocatalysis, Heliyon 7 (May) (2021), e08076.

[87] Shude Liu, K.S. Hui, K.N. Hui, Flower-like nopper cobaltite eanosheets on craphite paper as high-performance supercapacitor electrodes and nnzymeless Glucose sensors, ACS Appl. Mater. Interfaces 8 (5) (2016) 3258–3267.

[88] Lin Cheng, et al., NH4F assisted and morphology-gontrolled fabrication of ZnCo2O4 nanostructures on Ni-foam for enhanced energy storage devices, J. Alloys Compd. 781 (2019) 245–254.

[89] Faisal Ali, Nadeem R. Khalid, Ghulam Nabi, et al., Hydrothermal synthesis of eerium-doped Co3O4 canoflakes as electrode for supercapacitor application, Int. J. Energy Res. 45 (2) (2021) 1999–2010.

[90] Yi Zhou, et al., Controlled synthesis and characterization of nybrid Sn-doped Co3O4 canowires for supercapacitors, Mater. Lett. 216 (2018) 248–251.

[91] T. Priyadharshini, et al., Hexamine hole on pseudocapacitive nehaviour of cobalt oxide (Co 3 O 4) ranopowders, J. Nanosci. Nanotechnol. 18 (6) (2017) 4093–4099.

[92] P.M. Kharade, et al., Electrodeposited banoflakes like nydrophilic Co3O4 as a supercapacitor electrode, J. Phys. Chem. Solid. 120 (2018) 207–210.

[93] S.M. Jogade, D.S. Sutrave, Electrochemical performance of Mn doped Co3O4 supercapacitor: effect of nqueous electrolytes, J. Mater. Sci. Eng. 6 (3) (2017) 4–8.

[94] S. Kerli, Boron-doped cobalt oxide hhin ailms and its electrochemical properties, Mod. Phys. Lett. B 30 (27) (2016), 1650343.

[95] B. Jansi Rani, et al., Controlled synthesis and electrochemical properties of Ag-doped Co3O4 nanorods, Int. J. Hydrogen Energy 42 (50) (2017) 29666–29671.

[96] R.C. Ambare, S.R. Bharadwaj, B.J. Lokhande, Non-aqueous toute Spray fyrolyzed Ru:Co 3 O 4 rhin electrodes for supercapacitor application, Appl. Surf. Sci. 349 (2015) 887–896.

[97] Shaojuan Deng, et al., Cd doped porous Co3O4 panosheets as electrode material for high performance supercapacitor application, Electrochim. Acta 196 (2016) 316–327.

[98] Fuxiang Wei, et al., Controllable synthesis of tolyhedral Au@Co3O4 electrode for high performance supercapacitors, Mater. Lett. 255 (2019), 126534.
[99] Shanshan Li, et al., Hydrothermal synthesis of with nuperior plectroc Fe-doped Co3O4 srchin-like eicrostructureshemical performances, J. Alloys Compd. 821 (2020), 153507.
[100] Bhamini Bhujun, Michelle T.T. Tan, Anandan S. Shanmugam, Study of mixed uernary transition metal merrites as potential electrodes for supercapacitor applications, Results Phys. 7 (May) (2017) 345–353.
[101] Hongyan Gao, Shaokui Cao, Yan Cao, Hierarchical Core-Shell Nanosheet Arrays with MnO 2 Grown on Mesoporous CoFe 2 O 4 Support for High-Performance Asymmetric Supercapacitors, 2017.
[102] Xianbin Liu, et al., Highly tompressible three-fimensional craphene dydrogel for goldable all- holid-ftate supercapacitor, J. Power Sources 384 (November 2017) (2018) 214–222.
[103] Kangyu Zou, et al., Revealing dual capacitive mechanism of carbon cathode toward sltrafast suasi-uolid-qtate sithium ion capacitors, J. Energy Chem. 60 (2021) 209–221.
[104] Javed Iqbal, et al., Cobalt oxide sanograins and silver nanoparticles lecorated nibrous dolyaniline fanocomposite as pattery-type electrode for high performance nupercapattery, Polymers 12 (12) (2020) 1–19.